J. Fluid Mech. (1989), *vol.* 203, *pp.* 401–418
Printed in Great Britain

Steady compressible flow in collapsible tubes: application to forced expiration

By DAVID ELAD,[1] ROGER D. KAMM[2] AND ASCHER H. SHAPIRO[2]

[1] Biomedical Engineering Program, Faculty of Engineering, Tel Aviv University, Tel Aviv 69978, Israel

[2] Department of Mechanical Engineering, Massachusetts Institute of Technology, Cambridge MA 02139, USA

(Received 9 December 1987 and in revised form 8 December 1988)

Steady, one-dimensional flow of a compressible fluid through a collapsible tube is analysed. A general model is employed, incorporating axial variations in the parameters of the conducting system, such as the tube unstressed cross-section area and wall stiffness, the external pressure and energy exchange with the environment. The flow variables are described in differential form as functions of the conduit system parameters. A coupled set of equations for the dependent flow variables is summarized in a table of influence coefficients, which provides a clear and simple description of the effects produced by the system parameters. Examples of the effects of fluid compressibility in the respiratory system are presented for forced expiration manoeuvres. The effects are found to be generally small, but are most accentuated when breathing heavy gases and when the airways are pathologically stiffened.

1. Introduction

Flow through compliant tubes is usually treated as incompressible, even though the fluid may be a compressible gas. The one-dimensional theory of an incompressible fluid flow through a collapsible tube is already well established (Shapiro 1977), and is most often applied to physiological flows. While the assumption of fluid incompressibility is valid for blood or urine flows, the question arises whether it is sometimes not accurate for airflow in the bronchial network within the lung. In particular, fluid compressibility may be important in coughs or forced expiration manoeuvres, when air is rapidly expired from the lung. Pedersen *et al.* (1982, figure 11) induced forced expiration manoeuvres in mongrel dogs, and measured maximal flow rates of about 8 l/s at mid-trachea as well as cross-sectional areas of approximately 0.8 cm^2. These results indicate that the Mach number is approximately 0.3 at the flow limitation site (FLS). If the fluid downstream from the FLS is supercritical or passes though local non-uniformities (Elad, Kamm & Shapiro 1987), the Mach number may attain even higher values, in which case the effects of fluid compressibility may be important.

We present here a formulation for one-dimensional, steady flow of a perfect gas through a collapsible tube. The effects of the gas compressibility on the overall mechanical response of the fluid and tube is examined in lung models that, previously, have been analysed on the assumption of incompressibility (Elad *et al.* 1987; Elad, Kamm & Shapiro 1988*b*).

2. One-dimensional steady flow

2.1. *Assumptions of the model*

The cross-section of a collapsible tube exhibits a complex geometry when subjected to negative transmural (internal minus external) pressure. In general, the flow is then of a complicated three-dimensional nature. A common simplifying assumption in theoretical treatments of such flows, employed here, is that the flow is one-dimensional, with the fluid parameters averaged across the cross-section.

We assume that the following properties of the conducting tube vary along the axis of the tube: the unstressed ('resting') cross-sectional area, A_0; the elastic properties of the tube wall, represented by a stiffness parameter, K_p; and the pressure acting on the external wall of the tube, p_e. It is further assumed that the wavelength of longitudinal variations is much larger than the diameter of the tube, thus rendering transverse gradients negligible compared with longitudinal gradients. The flow is considered to be steady, fully developed, and in the turbulent range. Compressibility is taken into account by treating the flow as a perfect gas with fixed molecular weight W, and a constant specific heat c_p. Energy interchange with the outside or through latent heat effects is represented generally by axial variation of the stagnation temperature T_0; the flow is here assumed adiabatic, i.e. $\mathrm{d}T_0/\mathrm{d}x = 0$, except for a preliminary comparison with the isothermal case. Gravity is neglected.

2.2. *Governing equations and definitions*

Consider an infinitesimal control volume that consists of a section of the tube of length $\mathrm{d}x$. Several physical quantities are thought of as dependent variables, assumed continuously variable along x: the tube cross-sectional area A; and the cross-sectional-averaged values of fluid pressure p; velocity u; and density ρ.

Equation of state. For a perfect gas,

$$p = \rho RT; \quad \text{or} \quad \frac{\mathrm{d}p}{p} = \frac{\mathrm{d}\rho}{\rho} + \frac{\mathrm{d}T}{T}, \tag{1}$$

where T is the absolute temperature and R is the gas constant of the particular gas.

Fluid wave speed. The velocity of sound in a perfect gas is

$$c_F^2 = \gamma RT = \frac{\gamma p}{\rho}; \quad \text{or} \quad \frac{\mathrm{d}c_F^2}{c_F^2} = \frac{\mathrm{d}T}{T}, \tag{2}$$

where $\gamma = c_p/c_v$ is the ratio of the specific heats at constant pressure (c_p) and at constant volume (c_v).

Tube law. The 'tube law', relating the transmural pressure to the cross-sectional area of the tube at static conditions, is represented by

$$\Pi(\alpha, x) = \frac{p - p_e}{K_p(x)}, \tag{3}$$

where $p_e(x)$ is the external pressure, $\Pi(\alpha, x)$ is the dimensionless transmural pressure, and $\alpha = A/A_0$ is the dimensionless area ratio. Here, $A_0(x)$ is the unstressed cross-sectional area, and $K_p(x)$ is the tube stiffness parameter, both of which may vary with x.

Tube wave speed. The speed of propagation of long waves with infinitesimal area changes in compliant tubes is given by

$$c_T^2 = \frac{A}{\rho}\left(\frac{\mathrm{d}p}{\mathrm{d}A}\right)_x = \frac{K_p(x)}{\rho}\alpha\frac{\partial \Pi(\alpha, x)}{\partial \alpha}, \tag{4}$$

or in the differential forms

$$\mathrm{d}p = \mathrm{d}p_e + \rho c_T^2\frac{\mathrm{d}\alpha}{\alpha} + K_p\frac{\partial \Pi}{\partial x}\mathrm{d}x + \Pi\,\mathrm{d}K_p; \tag{5a}$$

$$\frac{\mathrm{d}c_T^2}{c_T^2} = \left(1+\alpha\frac{\Pi''}{\Pi'}\right)\frac{\mathrm{d}\alpha}{\alpha} + \frac{\mathrm{d}K_p}{K_p} + \frac{\alpha}{\rho}\frac{K_p}{c_T^2}\frac{\partial(\Pi')}{\partial x}\mathrm{d}x - \frac{\mathrm{d}\rho}{\rho}, \tag{5b}$$

where $\Pi' \equiv \partial\Pi/\partial\alpha$ and $\Pi'' \equiv \partial^2\Pi/\partial\alpha^2$.

Combined wave speed. Dynamically induced pressure changes produce corresponding area changes in the tube as well as density changes in the gas. These are related to the pressure change through the respective compliances: $(1/A)\,(\mathrm{d}A/\mathrm{d}p)$ and $(1/\rho)\,(\mathrm{d}\rho/\mathrm{d}p)$ which are recognized as the quantities $1/(\rho c_T^2)$ and $1/(\rho c_F^2)$, where the isentropic density derivative characterizes the gas compliance. Thus, the ratio

$$\frac{[(1/\rho)\,(\mathrm{d}\rho/\mathrm{d}p)]_{\mathrm{gas}}}{[(1/A)\,(\mathrm{d}A/\mathrm{d}p)]_{\mathrm{tube}}} = \frac{c_T^2}{c_F^2}$$

is a measure of the relative magnitudes of the two compliances. Moreover, since the compliances are effectively in series, the combined small-amplitude wave speed is given by (e.g. Lighthill 1978)

$$\frac{1}{c^2} = \frac{1}{c_T^2} + \frac{1}{c_F^2}; \quad \text{or} \quad \frac{1}{c^2}\frac{\mathrm{d}c^2}{c^2} = \frac{1}{c_T^2}\frac{\mathrm{d}c_T^2}{c_T^2} + \frac{1}{c_F^2}\frac{\mathrm{d}c_F^2}{c_F^2}. \tag{6}$$

For a gas, the stiffness (inverse compliance) is $c_F^2 = \gamma\bar{R}T/W$, where $\bar{R}$ denotes the universal gas constant and W the molecular weight. For an unstressed tube in partial collapse (i.e. under negative transmural pressure) the stiffness is proportional to the circumferential bending stiffness and is also strongly dependent on the degree of collapse. Thus, when $\alpha = O(1)$, the tube is relatively stiff against collapse; in the range $0.2 < \alpha < 0.8$ it is relatively compliant; while for $\alpha < 0.2$ it again becomes quite stiff. Typical comparative stiffness for several gas mixtures and airway generations at two particular lung volumes are given in table 1. The tube wave speed c_T^2 is calculated from the tube law we have developed for the airways (Elad, Kamm & Shapiro 1988*a*) at an area ratio of $\alpha = 0.7$.

In general, the gas mixtures are much stiffer than the airways, especially for lighter gas mixtures. These comparative stiffnesses determine the nature of the results shown later.

Mach number and speed index. The nature of compressible flow patterns depends on the comparative magnitudes of the fluid velocity and the speed of sound. A corresponding dependence applies to flow through collapsible tubes. The Mach number M and the speed index S are thus defined as

$$M = \frac{u}{c_F}; \quad \text{or} \quad \frac{\mathrm{d}M^2}{M^2} = \frac{\mathrm{d}u^2}{u^2} - \frac{\mathrm{d}c_F^2}{c_F^2}; \tag{7}$$

$$S = \frac{u}{c_T}; \quad \text{or} \quad \frac{\mathrm{d}S^2}{S^2} = \frac{\mathrm{d}u^2}{u^2} - \frac{\mathrm{d}c_T^2}{c_T^2}. \tag{8}$$

Airway	Trachea		Principal bronchus		Lobe bronchus		Bronchiole $d < 1$ mm		Terminal bronchiole	
	V_L (% TLC)		V_L (% TLC)		V_L (% TLC)		V_L (% TLC)		V_L (% TLC)	
Gas mixture	75.0	41.9	75.0	41.9	75.0	41.9	75.0	41.9	75.0	41.9
Air	13.4	19.6	28.6	41.8	38.6	56.4	57.9	84.5	76.3	111.7
$He–O_2$	15.4	22.5	32.8	48.0	44.3	64.9	66.6	97.3	87.7	128.2
$SF_6–O_2$	9.8	14.4	21.0	30.7	28.4	41.5	42.6	62.2	56.1	82.0

TABLE 1. Comparison between gas and tube stiffness (c_F^2/c_T^2) for three gas mixtures and several airway generations. c_T^2 is evaluated from the tube law previously developed (Elad *et al.* 1988*a*) at $\alpha = 0.7$. Lung volume $V_L = 41.9\%$ total lung capacity (TLC) is equivalent to $V_L = 25\%$ vital capacity (VC).

The combined speed index is then defined through

$$G^2 = \frac{u^2}{c^2} = \frac{u^2}{c_F^2} + \frac{u^2}{c_T^2} = M^2 + S^2. \tag{9}$$

Conservation of mass. In steady flow, mass conservation requires that

$$\rho u A = \text{constant}. \tag{10}$$

Introducing the area ratio α and differentiating, this may be written as

$$\frac{\mathrm{d}\rho}{\rho} + \frac{\mathrm{d}u}{u} + \frac{\mathrm{d}\alpha}{\alpha} + \frac{\mathrm{d}A_0}{A_0} = 0. \tag{11}$$

Momentum equation. For the infinitesimal control volume previously defined, the momentum equation is

$$-A\,\mathrm{d}p - \tau_w s\,\mathrm{d}x = \rho A u\,\mathrm{d}u, \tag{12}$$

where τ_w is the wall shear stress and s is the perimeter of the cross-section. As is customary, the skin-friction stress of a turbulent flow is expressed as $\tau_w \equiv f_T(\frac{1}{2}\rho u^2)$, where f_T, the skin-friction coefficient, is only a weak function of Reynolds number. The perimeter s = constant = πD_0 during collapse, where $D_0 = (4A_0/\pi)^{\frac{1}{2}}$ is the rest diameter. Then the equivalent hydraulic diameter is $D_e = 4A/s$; consequently $\alpha \equiv A/A_0 = D_e/D_0$. Thus, (12) becomes

$$\mathrm{d}p + \tfrac{1}{2}\rho u^2 \frac{4 f_T\,\mathrm{d}x}{D_e} + \rho u^2 \frac{\mathrm{d}u}{u} = 0, \tag{13}$$

or, with the help of (2) and (7)

$$\frac{\mathrm{d}p}{p} + \tfrac{1}{2}\gamma M^2 \frac{4 f_T\,\mathrm{d}x}{D_e} + \tfrac{1}{2}\gamma M^2 \frac{\mathrm{d}u^2}{u^2} = 0. \tag{14}$$

Energy equation. Changes in stagnation temperature T_0 are produced by heat exchange, chemical reactions, and phase change. For a perfect gas (Shapiro 1953)

$$T_0 = T + \frac{u^2}{2c_p} = T[1 + \tfrac{1}{2}(\gamma - 1)M^2], \tag{15}$$

which, after logarithmic differentiation, becomes

$$\frac{\mathrm{d}T_0}{T_0} = \frac{\mathrm{d}T}{T} + \frac{\frac{1}{2}(\gamma-1)M^2}{1+\frac{1}{2}(\gamma-1)M^2}\frac{\mathrm{d}M^2}{M^2}. \tag{16}$$

Except for a preliminary comparison with the isothermal limit, where $\mathrm{d}T/T = 0$, the numerical examples of this paper are based on the adiabatic limit.

2.3. *Differential equations and influence coefficients*

The set of nine equations (1), (2), (5*a*, *b*), (7), (8), (9), (11), (14) and (16) include seventeen differential variables. Seven of these, which define the conducting system and environmental conditions, may be chosen as independent variables. These independent variables are usually 'known' quantities which can be used to determine the dependent variables. In the present model the independent variables are: $\mathrm{d}A_0/A_0$, $\mathrm{d}T_0/T_0$, $4f_\mathrm{T}\,\mathrm{d}x/D_\mathrm{e}$, $\mathrm{d}p_\mathrm{e}$, $\mathrm{d}K_\mathrm{p}$, $(\partial\Pi/\partial\alpha)\,\mathrm{d}x$, and $[\partial(\partial\Pi/\partial\alpha)/\partial x]\,\mathrm{d}x$, while the dependent ones are: $\mathrm{d}\alpha/\alpha$, $\mathrm{d}u/u$, $\mathrm{d}p/p$, $\mathrm{d}\rho/\rho$, $\mathrm{d}T/T$, $\mathrm{d}c_\mathrm{F}^2/c_\mathrm{F}^2$, $\mathrm{d}c_\mathrm{T}^2/c_\mathrm{T}^2$, $\mathrm{d}M^2/M^2$, $\mathrm{d}S^2/S^2$, and $\mathrm{d}G^2/G^2$.

This set is a system of linear algebraic equations which can be solved simultaneously, so that each dependent variable is described in terms of the seven independent variables. For example, by elimination we obtain the following equations for $\mathrm{d}S^2/S^2$ and $\mathrm{d}M^2/M^2$:

$$\begin{aligned}(1-M^2-S^2)\frac{\mathrm{d}S^2}{S^2} = {} & [1+(\Gamma-1)(1-M^2)]\frac{\mathrm{d}p_\mathrm{e}}{\rho c_\mathrm{T}^2} + [-2+(2-\Gamma)S^2+M^2]\frac{\mathrm{d}A_0}{A_0} \\ & + [1+(\Gamma-1)S^2][1+\tfrac{1}{2}(\gamma-1)M^2]\frac{\mathrm{d}T_0}{T_0} \\ & + [\tfrac{1}{2}\Gamma S^2+\tfrac{1}{2}\gamma M^2+\tfrac{1}{2}(\Gamma-1)(\gamma-1)S^2M^2]\frac{4f_\mathrm{T}\,\mathrm{d}x}{D_\mathrm{e}} \\ & + \left[\Gamma-(\Gamma-1)M^2-(1-M^2-S^2)\frac{\rho c_\mathrm{T}^2}{\Pi K_\mathrm{p}}\right]\frac{\Pi}{\rho c_\mathrm{T}^2}\mathrm{d}K_\mathrm{p} \\ & + [\Gamma-(\Gamma-1)M^2]\frac{K_\mathrm{p}}{\rho c_\mathrm{T}^2}\frac{\partial\Pi}{\partial x}\mathrm{d}x - [1-M^2-S^2]\frac{\alpha K_\mathrm{p}}{\rho c_\mathrm{T}^2}\frac{\partial}{\partial x}\left[\frac{\partial\Pi}{\partial\alpha}\right]\mathrm{d}x; \end{aligned} \tag{17}$$

$$\begin{aligned}(1-M^2-S^2)\frac{\mathrm{d}M^2}{M^2} = {} & 2[1+\tfrac{1}{2}(\gamma-1)M^2]\frac{\mathrm{d}p_\mathrm{e}}{\rho c_\mathrm{T}^2} - 2[1+\tfrac{1}{2}(\gamma-1)M^2]\frac{\mathrm{d}A_0}{A_0} \\ & + (1+\gamma M^2+S^2)[1+\tfrac{1}{2}(\gamma-1)M^2]\frac{\mathrm{d}T_0}{T_0} + [\gamma M^2+S^2][1+\tfrac{1}{2}(\gamma-1)M^2] \\ & \times\frac{4f_\mathrm{T}\,\mathrm{d}x}{D_\mathrm{e}} + 2[1+\tfrac{1}{2}(\gamma-1)M^2]\frac{\Pi}{\rho c_\mathrm{T}^2}\mathrm{d}K_\mathrm{p} + 2[1+\tfrac{1}{2}(\gamma-1)M^2]\frac{K_\mathrm{p}}{\rho c_\mathrm{T}^2}\frac{\partial\Pi}{\partial x}\mathrm{d}x, \end{aligned} \tag{18}$$

where $\Gamma \equiv 3+\alpha\Pi''/\Pi'$.

Algebraic manipulation provides for all the dependent variables the *influence coefficients* that multiply the independent variables. These are summarized in table 2. For comparison with incompressible flow through collapsible tubes, the expression for $\mathrm{d}p$ is written

$$\begin{aligned}(1-M^2-S^2)\frac{\mathrm{d}p}{\rho u^2} = {} & -\frac{p_\mathrm{e}}{\rho c_\mathrm{T}^2} + \frac{\mathrm{d}A_0}{A_0} - [1+\tfrac{1}{2}(\gamma-1)M^2]\frac{\mathrm{d}T_0}{T_0} \\ & - \tfrac{1}{2}[1+(\gamma-1)M^2]\frac{4f_\mathrm{T}\,\mathrm{d}x}{D_\mathrm{e}} + \frac{\Pi}{\rho c_\mathrm{T}^2}\mathrm{d}K_\mathrm{p} - \frac{K_\mathrm{p}}{\rho c_\mathrm{T}^2}\frac{\partial\Pi}{\partial x}\mathrm{d}x. \end{aligned} \tag{19}$$

Dependent variables \ Independent variables	$\frac{dp_e}{\rho c_T^2}$	$\frac{dA_0}{A_0}$	$[1+\frac{1}{2}(\gamma-1)M^2]\frac{dT_0}{T_0}$
$(1-M^2-S^2)\frac{du}{u}$	1	-1	1
$(1-M^2-S^2)\frac{d\alpha}{\alpha}$	$-(1-M^2)$	S^2	$-S^2$
$(1-M^2-S^2)\frac{d\rho}{\rho}$	$-M^2$	M^2	$-(1-S^2)$
$(1-M^2-S^2)\frac{dT}{T}$	$-(\gamma-1)M^2$	$(\gamma-1)M^2$	$(1-\gamma M^2-S^2)$
$(1-M^2-S^2)\frac{dp}{p}$	$-\gamma M^2$	γM^2	$-\gamma M^2$
$(1-M^2-S^2)\frac{dS^2}{S^2}$	$1+(\Gamma-1)(1-M^2)$	$-2+(2-\Gamma)S^2+M^2$	$1+(\Gamma-1)S^2$
$(1-M^2-S^2)\frac{dM^2}{M^2}$	$2[1+\frac{1}{2}(\gamma-1)M^2]$	$-2[1+\frac{1}{2}(\gamma-1)M^2]$	$1+\gamma M^2+S^2)$
$(1-M^2-S^2)\frac{dG^2}{G^2}$	$2+\beta_T(\Gamma-1)$ $+[\beta_F(\gamma-1)-\beta_T(\Gamma-1)]M^2$	$-2+\beta_F(\gamma-1)M^2$ $+\beta_T[M^2+(2-\Gamma)S^2]$	$2+\beta_F(\gamma M^2+S^2-1)$ $+\beta_T[(\Gamma-1)S^2-1]$

TABLE 2. Influence coefficients for compressible flow through

The several expressions for the dependent variables represented by table 2 describe the flow patterns in terms of the conducting system parameters. By setting to zero all the influence coefficients, except for those in column below the independent variable that is of interest, one may also explore the several simple flows in which the effect of each independent variable on flow behaviour can be examined individually.

We note in (17), (18) and (19) that the comparative magnitudes of M^2 and S^2 determine the relative importance of gas compressibility and tube compliance, in accord with our earlier remarks concerning the ratio c_T^2/c_F^2.

2.4. *General features of flow patterns*

For negligible tube compliance, $c_T \to \infty$; hence $S \to 0$, and the influence coefficients in table 2 reduce to those for gas flow with constant specific heat and molecular weight. On the other hand, when fluid compressibility is negligible, $c_F \to \infty$; hence $M \to 0$, and table 2 then pertains to incompressible flow through collapsible tubes.

The equation for each dependent variable is generally of the form exhibited by $d\alpha/dx$:

$$\frac{d\alpha}{dx} = \frac{Y(\alpha, S^2, M^2, x)}{1-S^2-M^2}. \tag{20}$$

Thus, a singularity occurs at $G^2 = M^2+S^2 = 1$. Overlooking the fact that the one-dimensional approximation is weak there, all the dependent variables change at an infinite rate in this region. This is analogous to the case $M^2 = 1$ in gas dynamics, and to $S^2 = 1$ for incompressible flow through collapsible tubes (Shapiro 1977).

The case $G^2 = 1$ is possible mathematically, and is approximated physically, only in either of two circumstances: (i) $G^2 = 1$ occurs at the end of the tube; or (ii) at other

$\frac{4f_T\,dx}{D_e}$	$\frac{\Pi}{\rho c_T^2}dK_p$	$\frac{K_p}{\rho c_T^2}\frac{\partial \Pi}{\partial x}dx$	$\frac{\alpha K_p}{\rho c_T^2}\frac{\partial}{\partial x}\left[\frac{\partial \Pi}{\partial \alpha}\right]dx$
$\frac{1}{2}(\gamma M^2+\frac{1}{2}S^2)$	1	1	0
$-\frac{1}{2}S^2[1+(\gamma-1)M^2]$	$-(1-M^2)$	$-(1-M^2)$	0
$\frac{1}{2}M^2[(\gamma-1)S^2-\gamma]$	$-M^2$	$-M^2$	0
$-\frac{1}{2}(\gamma-1)M^2(\gamma M^2+S^2)$	$-(\gamma-1)M^2$	$-(\gamma-1)M^2$	0
$-\frac{1}{2}\gamma M^2[1+(\gamma-1)M^2]$	$-\gamma M^2$	$-\gamma M^2$	0
$\frac{1}{2}(\Gamma S^2+\gamma M^2+(\Gamma-1)(\gamma-1)S^2M^2)$	$\Gamma-(\Gamma-1)M^2-(1-M^2-S^2)\frac{\rho c_T^2}{\Pi K_p}$	$\Gamma-(\Gamma-1)M^2$	$-(1-M^2-S^2)$
$(\gamma M^2+S^2)[1+\frac{1}{2}(\gamma-1)M^2]$	$2[1+\frac{1}{2}(\gamma-1)M^2]$	$2[1+\frac{1}{2}(\gamma-1)M^2]$	0
$\{\gamma+\frac{1}{2}\beta_F[(\gamma-1)(\gamma M^2+S^2)-\gamma]\}M^2$ $+\{1+\frac{1}{2}\beta_T[(\Gamma-2+(\Gamma-1)(\gamma-1)M^2]\}S^2$	$2+\beta_F(\gamma-1)M^2$ $+\beta_T\left[-1+(\Gamma-1)(1-M^2)\right.$ $\left.-\frac{\rho c_T^2}{\Pi K_p}(1-S^2-M^2)\right]$	$2+\beta_F(\gamma-1)M^2$ $+\beta_T[-1+(\Gamma-1)(1-M^2)]$	$-\beta_F(1-M^2-S^2)$

collapsible tubes. $\beta_T=\left(\frac{c}{c_T}\right)^2=\frac{S^2}{S^2+M^2}$; $\beta_F=\left(\frac{c}{c_F}\right)^2=\frac{M^2}{S^2+M^2}$.

locations, there is a singularity of either saddle or nodal type at $G^2=1$, with the flow passing continuously through $G^2=1$ (Elad *et al.* 1987). The second type implies that the right-hand side of each of the differential equations for the dependent variables (e.g. $d\alpha/dx, \ldots$) is equal to 0/0. One finds that for $G^2=1$, the right-hand side of each differential equation in table 2 is a numerical multiple of

$$\left\{-\frac{1}{\rho c_T^2}\frac{dp_e}{dx}+\frac{1}{A_0}\frac{dA_0}{dx}-[1+\tfrac{1}{2}(\gamma-1)M^2]\frac{1}{T_0}\frac{dT_0}{dx}\right.$$
$$\left.-\tfrac{1}{2}[1+(\gamma-1)M^2]\frac{4f_T}{D_e}-\frac{\Pi}{\rho c_T^2}\frac{dK_p}{dx}-\frac{K_p}{\rho c_T^2}\frac{\partial \Pi}{\partial x}\right\}. \quad (21)$$

Thus, if this sum is zero for $G^2=1$, all the equations of table 2 simultaneously have a right-hand side of the form 0/0 and a saddle-type or nodal-type singularity exists. This allows a continuous transition through $G^2=1$ with a maximal flow rate for given upstream and environmental conditions. This is a case of flow limitation and the location where $G^2=1$ is the flow limitation site (FLS).

When there is a location where $G^2=1$, whether at the tube exit or before, the flow is described as a *critical* or *choked* flow. When $G^2<1$ the flow is *subcritical*, and when $G^2>1$ it is *supercritical*. Since the signs of the influence coefficients change at $G^2=1$, the effects of the independent variables are of opposite sense for subcritical and supercritical flows.

2.5. *Independent-variable functions used for calculations*

In the examples that follow, we simulate respiratory airflow through the airways. Accordingly, we assume the external pressure to be constant, hence $dp_e/dx=0$. We

also assume $dT_0/dx = 0$ although this is more difficult to justify. As gas accelerates through the narrowing airways, it cools owing to the increase in kinetic energy. Some heat is transferred to the gas from the walls, and, additionally, some moisture condensation may occur causing a release of latent heat. Both effects cause dT_0/dx to be positive and tend to produce a behaviour more like isothermal than adiabatic flow. We have performed the calculations described in the next section, assuming both limiting conditions: adiabatic and isothermal. We find that, while the peak Mach number is slightly greater if the flow is isothermal, the differences are relatively small, i.e. less than 3% for peak values of M or S. The functions $A_0(x)$, $K_p(x)$, and the value of f_T used for the examples are presented in Appendices A and B. We also define a dimensionless axial length $\xi = x/L$.

3. Flow limitation and forced expiration

Those physiological flows where fluid compressibility is most likely to play an important role include coughs and forced expiration manoeuvres. To assess the possible contribution of compressibility to flow patterns in the airways we apply the analysis of this paper to the lung-like model, free of compressibility, previously developed for investigation of choking phenomena (Elad *et al.* 1987). The model is briefly described in Appendix A. The entire expiration manoeuvre is treated as a series of quasi-steady flows at successively smaller lung volumes. The assumption of quasi-steadiness is justified by the fact that the characteristic time for a forced expiration is much larger than both the time required for waves to propagate along the bronchial tree and for fluid particles to traverse the conducting network. The fluid is assumed to be air at 37 °C with $\rho = 1.2\,\mathrm{kg/m^3}$, $\nu = 0.15\,\mathrm{cm^2/s}$ and $\gamma = 1.4$.

The equations of table 2 are coupled between themselves: terms of S and M appear in $d\alpha/dx$, terms of α and M in dS^2/dx, and so on. Thus, a simultaneous numerical solution is required. To illustrate the contribution of fluid compressibility for adiabatic and isothermal flows, numerical integrations have been performed for constant entrance conditions at $\xi = 0$, namely, $\alpha = 0.835$, $S = 0.3$, $Q = 2.3\,\mathrm{l/s}$, where Q is the flow rate computed at $\xi = 0$. The solid curves of figure 1 show $S(\xi)$ and $\alpha(\xi)$ for an incompressible fluid, i.e. $M = 0$. When the compressibility is such that $M = 0.1$ at $\xi = 0$, the curve of $S(\xi)$ is lifted, the curve of $M(\xi)$ rises to about 0.4 at $\xi = 1.0$, and the curve of $G(\xi)$ lies above $S(\xi)$. The peak values of M and S are about 3% greater for the isothermal flow while the general flow patterns are similar. Further increase of M to 0.13 at $\xi = 0$ drives the flow to choking (i.e. $G \to 1$ at $\xi = 0.17$ for isothermal flow and $\xi = 0.27$ for adiabatic flow). Unless the tube ends at that location, the assumed flow rate is physically impossible. The maximum allowable flow would be that combination of S and M at $\xi = 0$ that yields $G = 1$ at $\xi = 1.0$.

The determination of maximal flow by the present method requires that the singular saddle points be located. They may be found by setting expression (21) to be zero for any combination of $M^2 + S^2 = 1$. Figure 2 represents loci of such possible critical points for different combinations of $S^2 + M^2 = 1$. By expanding the equations for $d\alpha/d\xi$, $dM^2/d\xi$ and $dS^2/d\xi$ in a Taylor series, the values of α, S^2 and M^2, and their first derivatives, may be calculated at the critical point. Numerical integrations can proceed upstream and downstream.

Consider the case where $M^{*2} = 0.2$ and $S^{*2} = 0.8$ (the asterisks define a critical condition). The particular critical point that was chosen from the locus shown in figure 2 is the one that yields $\alpha = 1.0$ at $\xi = 0$, where bronchial pressure equals alveolar pressure ($p_{aw} = p_A$). The results for critical flow (or flow limitation) of

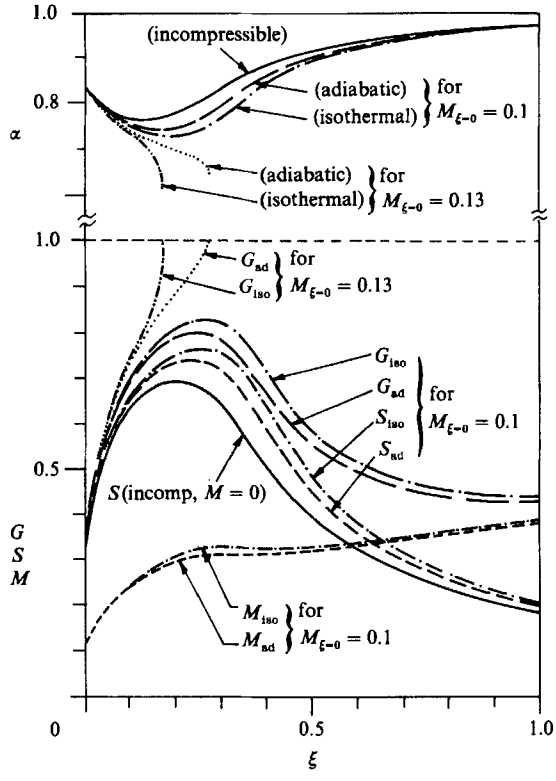

FIGURE 1. Example showing the contribution of fluid compressibility for subcritical, adiabatic and isothermal flows through the lung-like model (Appendix A), using different values for M at $\xi = 0$. All flows are for $\alpha = 0.835$ and $S = 0.3$ at $\xi = 0$. Solid curve, incompressible flow; other curves, compressible flow. The subscripts 'ad' and 'iso' stand for adiabatic and isothermal flow respectively.

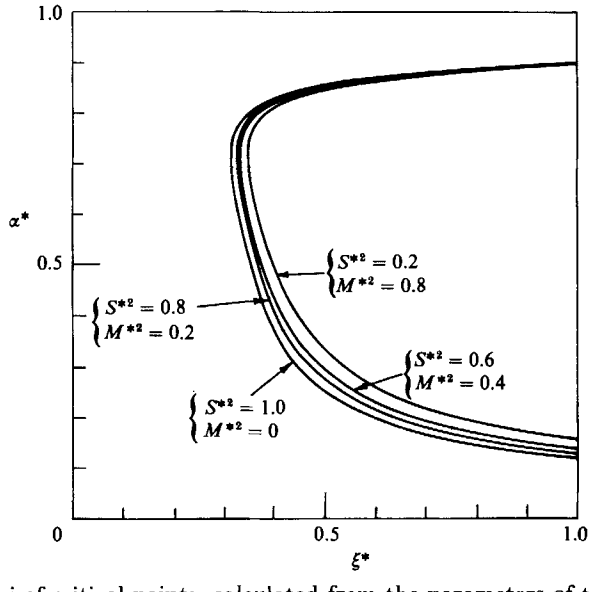

FIGURE 2. Loci of critical points, calculated from the parameters of the lung-like model (Appendix A), for different combinations of $M^{*2} + S^{*2} = 1.0$.

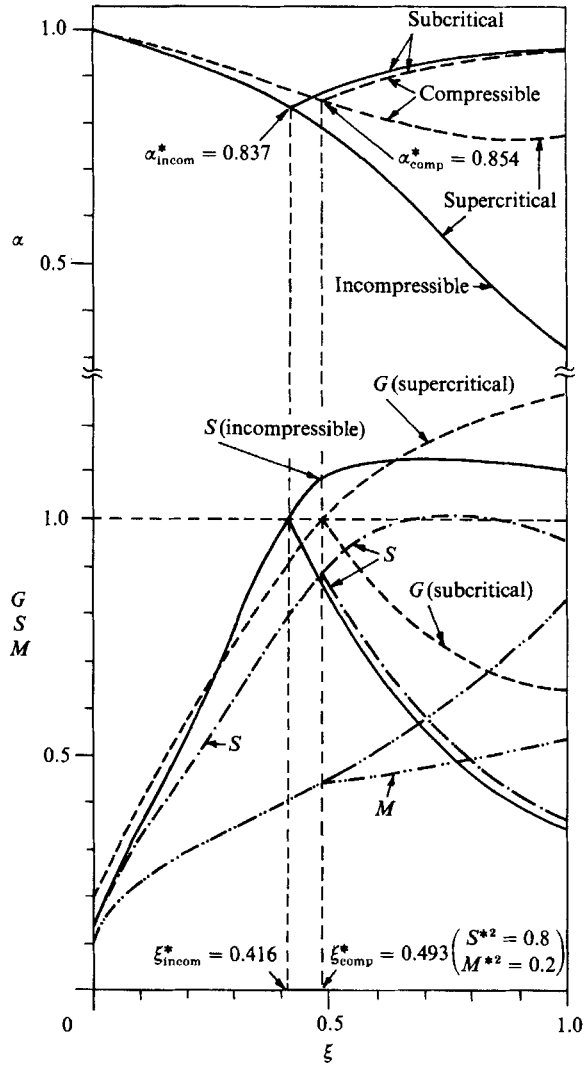

FIGURE 3. Patterns of critical flows through the lung-like model (Appendix A). All the flows are for $\alpha = 1.0$ at $\xi = 0$. The critical compressible flow yields $M^{*2} + S^{*2} = 1$ at the FLS.

incompressible and compressible fluids, both with $\alpha = 1.0$ at $\xi = 0$ and uniform p_e, are shown in figure 3. Table 3 compares some numerical values of these flows. Compressibility reduces the critical flow rate Q^* by about 8%, increases the area ratio at the FLS by about 2%, and moves the FLS further downstream by about 19%. Q^* was computed for both compressible and incompressible flows at $\xi = 0$ with the same ρ. The area ratios on the supercritical curve downstream of the FLS are much larger for compressible flows; accordingly, the transmural pressures are also higher. The collapsing transmural pressure at the bronchial outlet ($\xi = 1.0$) is about 3.6 times larger for compressible flows. The supercritical velocities downstream of the FLS are somewhat reduced by fluid compressiblity (e.g. $u = 19.4$ m/s versus $u = 27.0$ m/s at $\xi = 0.75$).

In physical terms, the effect of gas compressibility is to lend additional compliance to the system, thereby reducing the wave speed and, consequently, the flow speed at

Flow	α^*	ξ^*	Q^* [l/s]	$\alpha_{\xi=1.0}$ Sub-critical	$\alpha_{\xi=1.0}$ Super-critical	$(p-p_e)_{\xi=1.0}$ (cm H_2O) Sub-critical	$(p-p_e)_{\xi=1.0}$ (cm H_2O) Super-critical
Incompressible	0.837	0.416	3.636	0.9483	0.3296	−2.199	−15.776
Compressible	0.854	0.493	3.351	0.9566	0.7774	−1.962	−4.336

TABLE 3. Comparison between the flow parameters of the critical flows shown in figure 3. The inlet condition for both cases is determined by $\alpha = 1.0$ at $\xi = 0$.

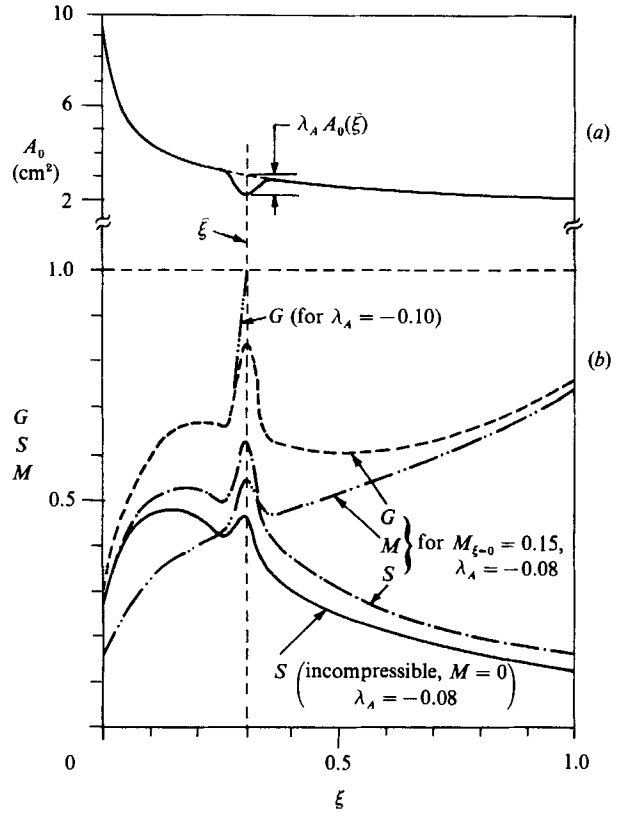

FIGURE 4. Flow pattern in the lung-like model with a local perturbation imposed on the natural cross-sectional area, A_0. (*a*) Perturbation in the rest area. (*b*) The effect on flow of different values of the perturbation parameter λ_A.

which flow limitation occurs. An additional effect is the reduction in gas density as M increases, further reducing the mass flow rate.

The movement of FLS downstream is somewhat counterintuitive but can be viewed in the following way. The two main features that influence the location of the FLS in these calculations are friction and the variation in airway stiffness as characterized by $dK_p/d\xi$; the FLS is established when these two effects are approximately balanced. If friction were progressively increased, we known from our experience with gas dynamic or collapsible-tube flow, that the FLS would move downstream, eventually reaching the end of the tube at which point a smooth transition to supercritical flow would no longer be possible. As seen from (21), the

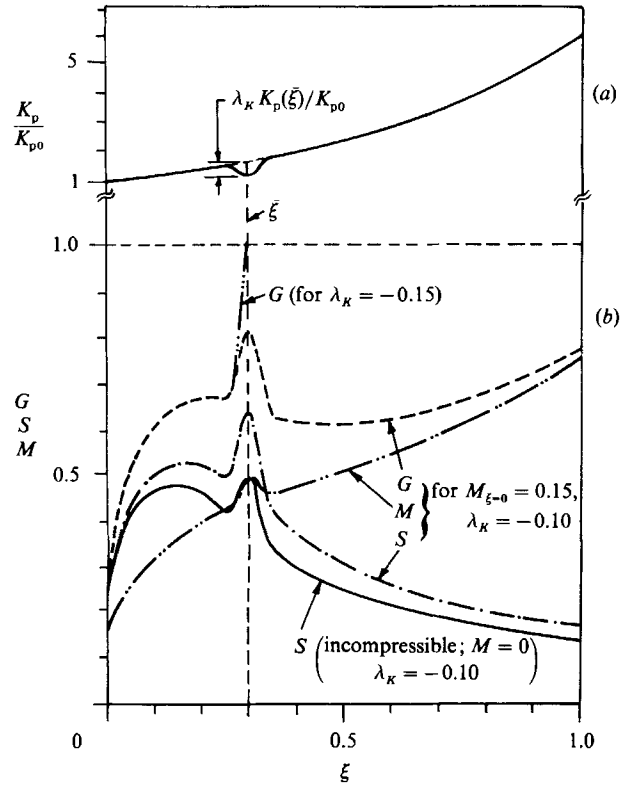

FIGURE 5. Flow pattern in the lung-like model with a local perturbation imposed on the tube wall stiffness, K_p. (*a*) Perturbation in the wall stiffness. (*b*) The effect on flow of different values of the peturbation parameter λ_K.

introduction of compressibility increases the importance of friction relative to that of stiffness variation, causing the FLS to move downstream to a location where $dK_p/d\xi$ is larger.

A similar result can be obtained for uniform tubes from the work of Grotberg & Shee (1985). Their expression for wave speed can be reduced, in a frictionless system with massless walls, to $c = c_T[1-\sigma^2+o(\sigma^4)]$, where $\sigma = c_T/c_F$. This reduction in wave speed also implies a reduction in limiting flow rate that scales with σ^2.

Earlier (Elad *et al.* 1987), we have shown that local reductions in the rest cross-sectional area (A_0) or wall stiffness (K_p), enhances the tendency for flow limitation. Figures 4 and 5 show how these tendencies are accentuated by compressibility. For example, while a local area decrease of 20% is required to drive an incompressible fluid flow toward flow limitation (Elad *et al.* 1987), a 10% decrease will suffice when fluid compressibility is considered with $M_{\xi=0} = 0.15$. A similar behaviour is also observed for local reductions in the tube wall stiffness.

4. Density dependence of maximum expiratory flow

Maximal expiratory flow is determined by the complex interaction between parenchymal elasticity, airway geometry, airway mechanics and physical properties of the expired gas mixture, especially its density. The gas mixtures that are often used in clinical assessments and physiological investigations are 80% helium with

20% oxygen ($He–O_2$), and 80% sulphur hexafluoride with 20% oxygen ($SF_6–O_2$) the properties of which are given in Appendix C. The maximal expiratory flow-volume curves for a particular normal subject, using different gas mixtures, are almost parallel to each other, especially in the range 40–70% vital capacity, where wave speed limitation occurs (Pedersen *et al.* 1982; Castile *et al.* 1983, 1986), with a lighter gas mixture yielding larger maximal expired flow rates. The $He–O_2$ mixture can be used for clinical evaluations of airways diseases, since the normal increase in maximal expired flow rate during $He–O_2$ breathing is not observed in patients with obstructions in the peripheral or central airways (Despas, Leroux & Macklem 1972; Dosman *et al.* 1975).

The effects of fluid compressibility for the different gas mixtures has been investigated by applying the present flow model to the more realistic lung model that we have developed earlier (Elad *et al.* 1988*b*), briefly described in Appendix B. With compressibility taken into account, the calculations are more complicated, since the density ρ is coupled with the variables of the right-hand side of the differential equations (table 2). Accordingly, numerical integration must be performed simultaneously for $d\alpha/\alpha$, dM^2/M^2, dS^2/S^2 and $d\rho/\rho$. To demonstrate the general trends of maximal expiration with different gas mixtures, we have carried out a complete calculation of the maximal expiratory flow rate for air, $He–O_2$ and $SF_6–O_2$ at 75% of total lung capacity. The critical point, where flow limitation occurs, was chosen by trial and error from different combinations of $M^{*2}+S^{*2} = 1.0$. The criterion for a critical point to be a FLS was that the following boundary conditions exist at the inlet ($\xi = 0$): (i) $p_{aw} = p_A$, and (ii) $M_{\xi=0} = (u/c_F)_{\xi=0}$, where $M_{\xi=0}$ is obtained by numerical integration from $\xi = \xi^*$ to $\xi = 0$, c_F is calculated from $\alpha_{\xi=0}$, and u is evaluated from Q^*. The results of the computations, for compressible and incompressible flows, are summarized in table 4. As before, the maximal flow rate is smaller for compressible flows, and the FLS is further downstream. However, the effects of fluid compressibility are small, perhaps immeasurably so, for all three mixtures.

A common measure used to compare the maximal expired flow rate of gas mixture to that of air at the same lung volume is density dependence. It is usually measured at 50% vital capacity and defined (for $He–O_2$ for example) as

$$DD_{50}^{He} = \frac{Q_{max}^{He-O_2}}{Q_{max}^{air}}. \tag{22}$$

In vivo measurements have shown that for normal human subjects $DD_{50}^{He} = 1.41 \pm 0.12$ (Castile, Hyatt & Rodarte 1980), while for normal mongrel dogs $DD_{50}^{He} = 1.55 \pm 0.13$ (Pedersen *et al.* 1982; Castile *et al.* 1983, 1986).

We used the numerical procedure to evaluate the density dependence for $He–O_2$ and $SF_6–O_2$. For this computation we assumed that $V_R = 22.5\%$ total lung capacity, as reported by Castile *et al.* (1980), and thus $\lambda = 1.75$ at $V_L = 50\%$ vital capacity = 61.25% total lung capacity. Here, V_R is the residual volume, V_L is any lung volume between $V_{L0} = 35\%$ and 100% total lung capacity, and $\lambda = V_L/V_{L0}$ is the lung volume ratio. From the results summarized in table 5, it is seen that compressibility scarcely affects the density dependence. The values of DD_{50}^{He} computed here are within the range of the observed measurements in normal humans. The computed results for both $He–O_2$ and $SF_6–O_2$, we note, are smaller than the square of the inverse ratio of the respective densities of the mixtures. This result is expected since the choking flow rate is dependent not only on the fluid density, but, as well, on cross-sectional area $(\alpha A_0)^*$ and wall stiffness at $\xi = \xi^*$. Since the location of the FLS is

	Air		$He–O_2$		$SF_6–O_2$	
	Incompressible	Compressible	Incompressible	Compressible	Incompressible	Compressible
α^*	0.4040	0.4054	0.3740	0.3752	0.4240	0.4332
ξ^*	0.6350	0.6855	0.6860	0.7490	0.6051	0.6365
S^*	1.0000	0.9721	1.0000	0.9720	1.0000	0.9670
M^*	0	0.2345	0	0.2349	0	0.2550
Q^* (l/s)	7.2334	7.1642	12.063	11.956	3.7030	3.6620
$\alpha_{\xi=0}$	1.2283	1.2285	1.2289	1.2290	1.2276	1.2286
$S_{\xi=0}$	0.0107	0.0106	0.0104	0.0103	0.0110	0.0108
$M_{\xi=0}$	0	0.0012	0	0.0011	0	0.0015

TABLE 4. Effects of compressibility on maximal expiratory flow in the lung model (Appendix B) at $V_L = 75\%$ total lung capacity, for three gas mixtures.

	Air		$He–O_2$ $\left[\frac{\rho_{air}}{\rho_{He-O_2}}\right]^{\frac{1}{2}} = 1.7244$		$SF_6–O_2$ $\left[\frac{\rho_{air}}{\rho_{SF_6-O_2}}\right]^{\frac{1}{2}} = 0.5011$	
	Incompressible	Compressible	Incompressible	Compressible	Incompressible	Compressible
DD_{50}	—	—	1.6456	1.6463	0.5164	0.5158
α^*	0.3927	0.3964	0.3540	0.3566	0.4168	0.4256
ξ^*	0.5683	0.5887	0.6290	0.6605	0.5379	0.5482
S^*	1.0000	0.9820	1.0000	0.9816	1.0000	0.9783
M^*	0	0.1889	0	0.1910	0	0.2074
Q^* (l/s)	5.7043	5.6612	9.3869	9.3202	2.9461	2.9198
$\alpha_{\xi=0}$	1.0576	1.0576	1.0576	1.0576	1.0576	1.0576
$S_{\xi=0}$	0.0115	0.0114	0.0110	0.0109	0.0118	0.0117
$M_{\xi=0}$	0	0.0012	0	0.0011	0	0.0014

TABLE 5. Effects of compressibility on maximal expiratory flow and density dependence at $V_L = 50\%$ vital capacity, for three gas mixtures.

different for the different gas mixtures, the flow-rate is not a function of the density ratio alone.

In the real lung model (Elad *et al.* 1988*b*) the trachea extends between $\xi = 0.548$ and $\xi = 1.0$. From table 5 we see that the FLS is located at 50% vital capacity in the trachea for all mixtures, as reported by Pedersen *et al.* (1982) and Castile *et al.* (1983, 1986). Castile *et al.* (1986) measured the cross-sectional area at the FLS and found it to be about 0.1 cm^2 smaller for $He–O_2$ than for air. For a typical trachea, this corresponds to $\Delta\alpha = 0.03–0.05$, in approximate agreement with our computations (table 5). The computed maximal flow rate for air at 50% vital capacity (5.66 l/s) is within the range of values measured by Castile *et al.* (1980, 1983, 1986).

Comparison between the patterns of compressible and incompressible critical flows (tables 4 and 5) indicates that incorporation of gas compressibility does not have a significant effect on the flow, in accordance with the comparative stiffness of the airways and the gas mixtures (table 1). Since the airway stiffness is directly related to the wall stiffness (K_p), we also examine the effect of wall stiffness on the flow pattern by multiplying $K_p(\xi)$ by a constant factor, β_{K_p}. In the absence of clinical

	Incompressible flow				Compressible flow			
β_{K_p}	0.5	1.0	2.0	5.0	0.5	1.0	2.0	5.0
Air								
α^*	0.3889	0.3927	0.3986	0.4057	0.3904	0.3964	0.4061	0.4255
ξ^*	0.5974	0.5683	0.5498	0.5351	0.6090	0.5887	0.5908	0.7882
S^*	1.0000	1.0000	1.0000	1.0000	0.9907	0.9820	0.9633	0.8503
M^*	0	0	0	0	0.1360	0.1889	0.2683	0.5263
Q^* (l/s)	4.1195	5.7043	8.0268	12.720	4.1042	5.6611	7.9075	12.297
$He–O_2$								
α^*	0.3374	0.3540	0.3710	0.3886	0.3396	0.3566	0.3747	0.3990
ξ^*	0.6879	0.6290	0.5884	0.5566	0.7049	0.6605	0.6545	0.8544
S^*	1.0000	1.0000	1.0000	1.0000	0.9899	0.9816	0.9616	0.8602
M^*	0	0	0	0	0.1414	0.1910	0.2744	0.5099
Q^* (l/s)	6.6830	9.3870	13.374	21.452	6.6589	9.3202	13.184	20.873
DD_{50}	1.6223	1.6456	1.6618	1.6864	1.6255	1.6464	1.6673	1.6973
$SF_6–O_2$								
α^*	0.4217	0.4168	0.4157	0.4166	0.4261	0.4258	0.4340	0.4666
ξ^*	0.5524	0.5379	0.5293	0.5228	0.5585	0.5484	0.5511	0.6285
S^*	1.0000	1.0000	1.0000	1.0000	0.9887	0.9778	0.9547	0.8573
M^*	0	0	0	0	0.1500	0.2098	0.2975	0.5148
Q^* (l/s)	2.1463	2.9461	4.1125	6.4656	2.1363	2.9186	4.0380	6.1724
DD_{50}	0.5210	0.5165	0.5123	0.5083	0.5205	0.5156	0.5107	0.5019

TABLE 6. Comparison of maximal expiratory flows at $V_L = 50\%$ vital capacity for different overall airways stiffnesses, and three gas mixtures.

β_{K_p}	0.5	1.0	2.0	5.0
Air				
$K_{p0}/\rho c_F^2$	0.0060	0.0120	0.0210	0.0601
$\bar{Q}$	0.0037	0.0076	0.0149	0.0333
$He–O_2$				
$K_{p0}/\rho c_F^2$	0.0052	0.0104	0.0209	0.0522
$\bar{Q}$	0.0036	0.0071	0.0142	0.0270
$SF_6–O_2$				
$K_{p0}/\rho c_F^2$	0.0082	0.0163	0.0327	0.0817
$\bar{Q}$	0.0047	0.0093	0.0181	0.0453

TABLE 7. Effects of different airway stiffnesses on the comparative ratio $\bar{Q} = (Q^*_{\text{incomp}} - Q^*_{\text{comp}})/Q^*_{\text{incomp}}$. Evaluated for the numerical results of table 6.

information concerning the extent of change in airway stiffness in diseases such as emphysema or pulmonary fibrosis, we assume several values for β_{K_p} between 0.5 and 5.0. Values of critical flows at $V_L = 50\%$ vital capacity for three gas mixtures with several airways stiffnesses (represented by β_{K_p}) are summarized in table 6. The results show that increased wall stiffness increases the flow rate, but the difference between incompressible and compressible flow rates remains very small. However, increased wall stiffness increases the differences in the flow pattern, as indicated by the cross-sectional-area ratio (α^*) and location (ξ^*) of the FLS, as well as the values and distribution of S and M.

Analysis of the values of flow rate in table 6 shows that a dimensionless parameter such as $K_{p0}/\rho c_F^2$, where $K_{p0} = K_p$ ($\xi = 0$), may be used as an indication of the effect

of compressibility on the critical flow rate (or flow limitation). We define the ratio $\bar{Q} \equiv (Q^*_{\text{incomp}} - Q^*_{\text{comp}})/Q^*_{\text{incomp}}$ to represent the difference between incompressible and compressible flow rates. We find that changes in $\bar{Q}$ scale within changes in the dimensionless grouping c_T^2/c_F^2 which we represent by $K_{p0}/\rho c_F^2$. As shown in table 7 the ratio of $\bar{Q}$ to $K_{p0}/\rho c_F^2$ (for results of table 6) falls between the values of 1.4 and 2.0 for the simulations presented here.

5. Conclusions

This study examines the effects of gas compressibility on flow patterns in collapsible tubes with particular emphasis on forced expiration manoeuvres. Applied to lung models, the results show that compressibility does affect the flow pattern but has only a small influence on the flow rate. The most significant effect is the movement of the FLS to a location further downstream. This downstream movement is increased for lungs with stiffer airways. In cases with local non-uniformities in the airway cross-sectional area or wall stiffness, compressibility can more significantly enhance the tendency of the flow to reach flow limitation.

This work was partially supported by the NHLBI (grant no. P01-HL-33009). Dr D. Elad is presently a Bat-Sheva de Rothschild Fellow.

Appendix A. Lung-like model (Elad *et al.* 1987)

The bronchial tree is considered symmetric, and its geometry is described by the number and total cross-sectional area of bronchi represented by smooth and continuous functions of distance along the airway system (see Elad *et al.* 1987, figure 1). The geometry of the first 10 generations of Weibel's (1963) measurements are well described by the rest area, which is expressed by $A_0(\xi) = 2.26(\xi+0.01)^{-0.3}$ cm^2, and the number of bronchi, which is expressed by $N(\xi) = 1.04(\xi+0.01)^{-1.36}$, where $\xi = x/L$ is non-dimensional length and the overall length of the airway system is $L = 18.4$ cm. The airway stiffness is represented by a single similarity tube law, $\Pi = (p_{aw}-p_A)/K_p = \alpha^{20.0}-\alpha^{-1.5}$, for the entire range of deformation ($\alpha > 1.0$ for inflation, and $\alpha < 1.0$ for deflation). The alveolar pressure (p_A) is the pressure acting on the external wall of the airways, while the airway pressure (p_{aw}) is the local internal fluid pressure. The wall stiffness variation along the bronchial tree is assumed to be given by $K_p(\xi) = 50\exp(1.8\xi)$ N/m^2. The fluid flow is assumed one-dimensional. The wall shear stress is represented using a turbulent friction coefficient of $f_T = 0.005$.

Appendix B. Real lung model (Elad *et al.* 1988*a*, *b*)

This model is similar in principle to the lung-like model (Elad *et al.* 1987), but has more realistic parameters. The bronchial tree is considered symmetric and includes the 17 generations of conducting airways, defined by Weibel (1963) from a human lung inflated to 75% total lung capacity. The total rest area of the cross-sections is given by $A_0(\xi) = 2.33(\xi+0.01)^{-0.9} - 14.0\exp(-3.98\xi)$ cm^2 and the number of branches by $N(\xi) = 1.04(\xi+0.01)^{-2.4} - 20.0\exp(-5.98\xi)$, where $\xi = x/L$ and $L = 26.5$ cm (Elad *et al.* 1988*b*).

The similarity tube law for the airways is considered to be lung-volume (V_L) dependent, and is given by $\Pi = (p_{aw}-p_A-p_0)/K_p = \alpha^{0.5}-\alpha^{-0.2}$, where $\alpha = A/A_0(\lambda)$, $A_0(\lambda) = 0.92A_0(\xi)[1.0+0.0135(\lambda^{2.7}-1)]$ cm^2, $K_p(\lambda) = 16.7\exp(2.4\xi)$

Gas mixture	ρ (kg/m^3)	$\mu \times 10^5$ (kg/m s)	ν (cm^2/s)	γ	c_F (m/s)
Air	1.13	1.9	0.168	1.400	353.0
He–O_2	0.38	2.1	0.550	1.588	652.9
SF_6–O_2	4.50	1.6	0.035	1.100	151.7

TABLE 8. Physical constants of gas mixtures at 37 °C and atmospheric conditions.

$[1.0+0.078(\lambda^{2.7}-1)]$ cm H_2O, $p_0(\lambda) = -0.0136(\lambda^{7.4}-1)$ cm H_2O and $\lambda = V_L/V_{L0}$ is the lung-volume ratio. $V_{L0} = 35\,\%$ total lung capacity is assumed to be the unstressed lung volume (Elad *et al.* 1988*a*).

The flow is considered one-dimensional, where the wall shear stress expressed as $\tau_w = \frac{1}{2}\rho u^2 f_T$. The friction coefficient is assumed to be of the form $f_T = 16(1.5+0.0013Re)/Re$, where $Re = uD_e/\nu$ is the Reynolds number.

Appendix C. Properties of gas mixtures

Previous investigators (Castile *et al.* 1980, 1983, 1986; Pedersen *et al.* 1982; Pedersen & Ingram 1985; Isabey & Chang 1981; Lambert 1986; Mink, Ziesmann & Wood 1979; Wood *et al.* 1976) used the following values for the density ρ of the gas mixtures: 1.07–1.13 kg/m^3 for air, 0.372–0.44 kg/m^3 for He–O_2, and 4.27–4.58 kg/m^3 for SF_6–O_2. For the viscosity coefficient μ they used: $1.87–1.89 \times 10^{-5}$ kg/(m s) for air, $2.10–2.26 \times 10^{-5}$ kg/(m s) for He–O_2 and $1.60–1.62 \times 10^{-5}$ kg/(m s) for SF_6–O_2.

The gas mixture is assumed dry, since water vapour and CO_2 have negligible effects on γ and c_F in the physiological range (Visser 1979). We assume atmospheric conditions at 37 °C and take the values for air (78 % N_2, 21 % O_2, 1 % CO_2 and H_2O) from Ower & Parkhurst (1977). For the gas mixtures of He–O_2 and SF_6–O_2, we corrected slightly the ratios with respect to air that were measured by Isabey & Chang (1981) at 20 °C. The results are summarized in table 8. The kinematic viscosity is given by $\nu = \mu/\rho$.

The ratio of specific heats γ and the velocity of sound c_F for a given gas mixture can be determined by the molar quantities of the mixtures subject to the ideal-gas assumption (Visser 1979). The mean molar mass of a gas mixture is

$$\bar{M} = \sum_i x_i M_i, \tag{C 1}$$

where i is the number of gas components and x_i is the fraction of gas i in the mixture ($\sum x_i = 1.0$). The mean ratio of specific heats for a gas mixture can be evaluated (Visser 1979) with good accuracy (within 2–3 % of tabulated data for water vapour, nitrous oxide and carbon dioxide) from the following empirical equation:

$$\bar{\gamma} = 1 + \frac{12}{\sum_i x_i(4+15N_i-N_i^2)}, \tag{C 2}$$

were N_i is 1 for monoatomic gases, 2 for diatomic gases, and 3 for tri- or polyatomic gases. The velocity of sound of the gas mixture is given by

$$c_F^2 = \bar{\gamma}\frac{\bar{R}}{\bar{M}}T, \tag{C 3}$$

where $\bar{R} = 8314.3$ J/kg mol °K is the universal gas constant.

Following (C 1), (C 2) and (C 3), one can calculate $\bar{\gamma}$ and c_F for any gas mixture, and the results for air, $He–O_2$ and $SF_6–O_2$ are summarized in table 8. SF_6 is a relatively complex molecule, thus we assume *a priori* that $\bar{\gamma}_{SF_6} = 1.05$. Since the empirical relations for $\bar{\gamma}$ (equation (C 2)) do not apply to complex molecules, we further assume that for the mixture $SF_6–O_2$, $\bar{\gamma} = 1.10$.

REFERENCES

CASTILE, R. G., HYATT, R. E. & RODARTE, J. R. 1980 Determinants of maximal expiratory flow and density dependence in normal humans. *J. Appl. Physiol.* **49**, 897–904.

CASTILE, R. G., PEDERSEN, O. F., DRAZEN, J. M. & INGRAM, R. H. 1983 Density dependence of maximal flow in dogs with central and peripheral obstruction. *J. Appl. Physiol.* **55**, 717–725.

CASTILE, R. G., PEDERSEN, O. F., DRAZEN, J. M. & INGRAM, R. H. 1986 Density dependence of maximal expiratory flow before and during tracheal constriction in dogs. *J. Appl. Physiol.* **60**, 1060–1066.

DESPAS, P. J., LEROUX, M. & MACKLEM, P. T. 1972 Site of airway obstruction in asthma as determined by measuring maximal expiratory flow breathing air and helium–oxygen mixture. *J. Clin. Invest.* **51**, 3235–3243.

DOSMAN, J., BODE, F., URBANETTI, J., MARTIN, R. & MACKLEM, P. T. 1975 The use of helium–oxygen mixture during maximum expiratory flow to demonstrate obstruction in small airways in smokers. *J. Clin. Invest.* **55**, 1090–1099.

ELAD, D., KAMM, R. D. & SHAPIRO, A. H. 1987 Choking phenomena in a lung-like model. *Trans. ASME* K: *J. Biomech. Engng* **109**, 1–9.

ELAD, D., KAMM, R. D. & SHAPIRO, A. H. 1988*a* Tube-law for the intrapulmonary airway. *J. Appl. Physiol.* **65**, 7–13.

ELAD, D., KAMM, R. D. & SHAPIRO, A. H. 1988*b* Mathematical simulation of forced expiration *J. Appl. Physiol.* **65**, 14–25.

GROTBERG, J. B. & SHEE, T. R. 1985 Compressible-flow channel flutter. *J. Fluid Mech.* **159**, 175–193.

ISABEY, D. & CHANG, H. K. 1981 Steady and unsteady pressure–flow relationships in central airways. *J. Appl. Physiol.* **51**, 1338–1348.

LAMBERT, R. K. 1986 Analysis of bronchial mechanics and density dependence of maximal expiratory flow. *J. Appl. Physiol.* **61**, 138–149.

LIGHTHILL, M. J. 1978 *Waves in Fluids*, chap. 2. Cambridge University Press.

MINK, S., ZIESMANN, M. & WOOD, L. D. H. 1979 Mechanisms of increased maximum expiratory flow during HeO_2 breating in dogs. *J. Appl. Physiol.* **47**, 490–502.

OWER, E. & PANKHURST, P. C. 1977 *The Measurement of Air Flow*, chap. 5. Pergamon.

PEDERSEN, O. F., CASTILE, R. G., DRAZEN, J. M. & INGRAM, R. H. 1982 Density dependence of maximum expiratory flow in the dog. *J. Appl. Physiol.* **53**, 397–404.

PEDERSEN, O. F. & INGRAM, R. H. 1985 Configuration of the maximal expiratory flow-volume curve: model experiments with physiological implications. *J. Appl. Physiol.* **58**, 1305–1313.

SHAPIRO, A. H. 1953 *The Dynamics and Thermodynamics of Compressible Fluid Flow*, vol. I. New York: Ronald.

SHAPIRO, A. H. 1977 Steady flow in collapsible tubes. *Trans. ASME* K: *J. Biomech. Engng* **99**, 126–147.

VISSER, B. F. 1979 Velocity of sound in gas mixtures. *Prog. Resp. Res.* **11**, 224–234.

WEIBEL, E. R. 1963 *Morphology of the Human Lung*. Academic.

WOOD, L. D. H., ENGEL, L. A., GRIFFIN, P., DESPAS, P. & MACKLEM, P. T. 1976 Effect of gas physical properties and flow on lower pulmonary resistance. *J. Appl. Physiol.* **41**, 234–244.